

TiO_2 composite electron transport layers for planar perovskite solar cells by mixed spray pyrolysis with precursor solution incorporating TiO_2 nanoparticles

Jiaqi Tian(田嘉琪), Hongcui Li(李红翠), Haiyue Wang(王海月), Bo Zheng(郑博), Yebin Xue(薛叶斌), Xizhe Liu(刘喜哲)
Citation: Chin. Phys. B . 2018, 27(1): 018810. **doi:** 10.1088/1674-1056/27/1/018810

Journal homepage: http://cpb.iphy.ac.cn; http://iopscience.iop.org/cpb

What follows is a list of articles you may be interested in

Efficient design of perovskite solar cell using mixed halide and copper oxide

Navneet kour, Rajesh Mehra, Chandni
Chin. Phys. B . 2018, 27(1): 018801. **doi:** 10.1088/1674-1056/27/1/018801

TiO_2 composite electron transport layers for planar perovskite solar cells by mixed spray pyrolysis with precursor solution incorporating TiO_2 nanoparticles

Jiaqi Tian(田嘉琪), Hongcui Li(李红翠), Haiyue Wang(王海月), Bo Zheng(郑博), Yebin Xue(薛叶斌), Xizhe Liu(刘喜哲)
Chin. Phys. B . 2018, 27(1): 018810. **doi:** 10.1088/1674-1056/27/1/018810

O_3 fast and simple treatment-enhanced p-doped in Spiro-MeOTAD for CH_3NH_3I vapor-assisted processed $CH_3NH_3PbI_3$ perovskite solar cells

En-Dong Jia(贾恩东), Xi Lou(娄茜), Chun-Lan Zhou(周春兰), Wei-Chang Hao(郝维昌), Wen-Jing Wang(王文静)
Chin. Phys. B . 2017, 26(6): 068803. **doi:** 10.1088/1674-1056/26/6/068803

Simulation design of P-I-N-type all-perovskite solar cells with high efficiency

Hui-Jing Du(杜会静), Wei-Chao Wang(王韦超), Yi-Fan Gu(顾一帆)
Chin. Phys. B . 2017, 26(2): 028803. **doi:** 10.1088/1674-1056/26/2/028803

Device simulation of lead-free $CH_3NH_3SnI_3$ perovskite solar cells with high efficiency

Hui-Jing Du(杜会静), Wei-Chao Wang(王韦超), Jian-Zhuo Zhu(朱键卓)
Chin. Phys. B . 2016, 25(10): 108802. **doi:** 10.1088/1674-1056/25/10/108802

SPECIAL TOPIC — New generation solar cells

TiO_2 composite electron transport layers for planar perovskite solar cells by mixed spray pyrolysis with precursor solution incorporating TiO_2 nanoparticles*

Jiaqi Tian(田嘉琪)#, Hongcui Li(李红翠)#, Haiyue Wang(王海月), Bo Zheng(郑博), Yebin Xue(薛叶斌), and Xizhe Liu(刘喜哲)†

Institute of Atomic and Molecular Physics, Jilin Provincial Key Laboratory of Applied Atomic and Molecular Spectroscopy, Jilin University, Changchun 130012, *China*

(Received 29 September 2017; revised manuscript received 16 November 2017; published online 22 December 2017)

Perovskite solar cells with planar structure are attractive for their simplified device structure and reduced hysteresis effect. Compared to conventional mesoporous devices, TiO_2 porous scaffold layers are removed in planar devices. Then, compact TiO_2 electron transport layers take the functions of extracting electrons, transporting electrons, and blocking holes. Therefore, the properties of these compact TiO_2 layers are important for the performance of solar cells. In this work, we develop a mixed spray pyrolysis method for producing compact TiO_2 layers by incorporating TiO_2 nanoparticles with different size into the precursor solutions. For the optimized nanoparticle size of 60 nm, a power conversion efficiency of 16.7% is achieved, which is obviously higher than that of devices without incorporated nanoparticles (9.9%). Further investigation reveals that the incorporation of nanoparticles can remarkably improve the charge extraction and recombination processes.

Keywords: perovskite solar cell, electron transport layer, charge extraction, recombination

PACS: 88.40.H–, 88.40.hj, 73.63.–b **DOI:** 10.1088/1674-1056/27/1/018810

1. Introduction

Perovskite solar cells have become a promising candidate for low-cost photovoltaic applications. In the past five years, the power conversion efficiency (PCE) of these devices has increased from 3.8% to 22.1%.[1–7] The excellent performance is partly related to the effective charge separation at the interface between the electron transport layers and light harvester layers.[8] Therefore, the properties of electron transport layers are important for the performance of perovskite solar cells.

Several types of materials can be used for fabricating electron transport layers, such as TiO_2,[9,10] ZnO,[11,12] SnO_2,[13,14] and $PC_{61}BM$.[15,16] Among these materials, TiO_2 has been widely used in the perovskite solar cells with conventional device structure, owing to its suitable energy band structure and electron mobility.[17,18] Although mesoporous TiO_2 layers can facilitate the electron collection at the TiO_2/perovskite interfaces, planar perovskite solar cells without mesoporous layers receive much attention for their simple device structure and reduced hysteresis effect.[19,20]

As electron transport layers have the functions of electron extraction and transport, their transport properties directly affect the performance of perovskite solar cells. The TiO_2 electron transport layers are widely deposited by spray pyrolysis or spin-coating of $Ti(OPr)_4$ precursor solutions.[21,22] These solution deposition methods are cost-effective and scalable, but the deposited TiO_2 layers usually have an amorphous structure, which is harmful to the efficient transport of electrons.[23] The slow electron transport can lead to enhanced recombination, especially for planar devices fabricated by two-step methods.[24] Therefore, modification methods of TiO_2 electron transport layers have been investigated to improve these planar devices.[25,26]

TiO_2 nanoparticles have been widely investigated for their photoelectric and catalysis properties,[27] and the size and crystallization of these materials can be conveniently controlled in large-scale synthesis.[27] Incorporating TiO_2 nanoparticles into the amorphous TiO_2 layers may provide additional transport channels for electrons in the electron transport layers, and the length of these channels can be easily controlled by the size of nanoparticles. Although TiO_2 nanoparticles have been applied for producing mesoporous layers in perovskite solar cells, these layers work as the scaffold of perovskite layers in the mesoporous devices, which have different functions from the compact TiO_2 layers of planar devices.[28]

In this work, we develop composite TiO_2 electron transport layers by a mixed spray pyrolysis method. TiO_2 nanoparticles are incorporated into the $Ti(OPr)_4$ precursor solutions,

*Project supported by the National Natural Science Foundation of China (Grant Nos. 51772125 and 51273079) and the Science Development Program of Jilin Province, China (Grant No. 20150519021JH).

#J. Tian and H. Li contributed equally.

†Corresponding author. E-mail: liu_xizhe@jlu.edu.cn

© 2018 Chinese Physical Society and IOP Publishing Ltd

and the properties of these composite layers are characterized. By optimizing the size of the nanoparticles, the performance of planar perovskite solar cells with different composite TiO_2 layers are investigated.

2. Experiment

For producing perovskite solar cells, fluorine-doped tin oxide (FTO) glass substrates were etched by 1064 nm laser and cleaned by acetone, ethanol, and deionized water in ultrasonic bath, sequentially. Then, TiO_2 electron transport layers were deposited by spray pyrolysis with 2.0 mL 0.05 M $Ti(OPr)_2(acetylacetonate)_2$ in ethanol solution at 450 °C. For incorporating TiO_2 nanoparticles into the TiO_2 layers, 4.0 mg/mL nanoparticles were ultrasonically dispersed in the 0.05 M $Ti(OPr)_2(acetylacetonate)_2$/ethanol solution. Three types of nanoparticles, with sizes of 25 nm, 60 nm, and 100 nm were employed, which are labeled to 25 nm NPs, 60 nm NPs, and 100 nm NPs. PbI_2 layers were deposited on TiO_2 compact layers by spin-coating at 4000 rpm for 30 s with 462 mg/mL PbI_2 in *N*,*N*-dimethylformamide (DMF) solution. After drying at 70 °C for 5 min, 0.4 mL 10 mg/mL CH_3NH_3I in isopropanol solution was sprayed on the top of PbI_2 layers at 80 °C.[29] Next, the perovskite films were annealed at 100 °C for 30 min, and they were cleaned with isopropanol solution twice. Then, the samples were annealed on a hot plate at 70 °C for an additional 30 min. When cooled to room temperature, hole transport material (HTM) layers were prepared by spin-coating a solution containing 72.3 mg spiro-MeOTAD, 28.8 μL 4-tert-butylpyridine, and 17.5 μL lithium bis(trifluoromethanesulfonyl)imide solution (520 mg/mL in acetonitrile) in 1 mL chlorobenzene solvent at 4000 rpm for 20 s. Finally, Ag electrodes were deposited on the HTM layers by vacuum thermal evaporation.

Scanning electron microscopy (SEM) images were obtained using a FEI-MAGELLAN 400 scanning electron microscope. X-ray diffraction (XRD) patterns were obtained using a Rigaku D/max-2550 x-ray diffractometer. Photocurrent density–photovoltage characteristics were recorded from 1.15 V to 0 V by a CHI660 electrochemical workstation. The active area of solar cells is 0.15 cm^2, which was defined by a mask. AM1.5 illumination was provided by a 3A class solar simulator (UHE-16, ScienceTech Inc.), which was calibrated to one sun by a KG5 filtered Si reference solar cell (certificated by VLSI Standards Inc., traceable to National Renewable Energy Laboratory). IPCE spectra were measured in the DC mode by a controlled monochrometer (BOCIC Inc.), and a calibrated Si cell was used as the reference. Photoluminescence (PL) spectra were detected by a CCD detector (PIXIS256BR, Princeton Instruments Inc.), and the excitation wavelength was 532 nm provided by a low-noise solid state laser (MLL-III-532). Impedance spectra were measured under constant illumination condition over a frequency range from 1 MHz to 1 Hz using a CHI660 electrochemical workstation.

3. Results and discussion

Figure 1 shows the SEM morphology of TiO_2 electron transport layers, which are deposited by the precursor solutions without and with different nanoparticles. For the TiO_2 layers deposited by the precursor solution without nanoparticles in Fig. 1(a), the surface preserves the morphology of FTO layers and the TiO_2 layers smoothly cover the surface of FTO layers.[30] By incorporating 25 nm TiO_2 nanoparticles in the precursor solutions, the surface roughness of TiO_2 layers increases (Fig. 1(b)). The rough surface reflects the existence of these nanoparticles in the TiO_2 layers. For the TiO_2 layers incorporating 60 nm nanoparticles, the morphology of FTO layers is still largely preserved (Fig. 1(c)). However, large particle clusters emerge in the TiO_2 layers incorporating 100 nm TiO_2 nanoparticles (Fig. 1(d)). As shown in Fig. 1, the surface roughness of TiO_2 layers continuously increases with the increase in nanoparticle size.

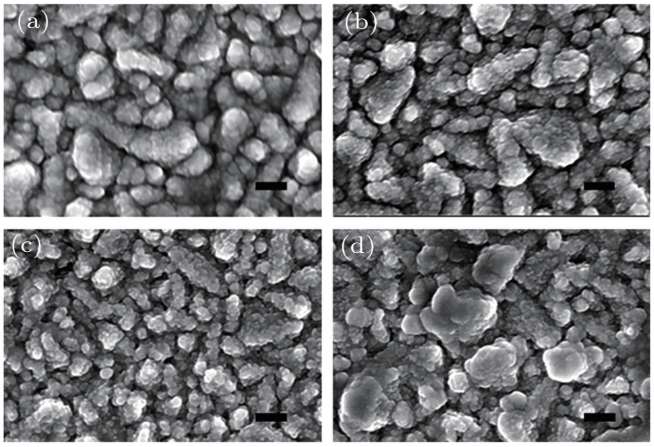


Fig. 1. Surface morphology of TiO_2 layers without (a) and with incorporation of 25 nm (b), 60 nm (c), and 100 nm (d) TiO_2 nanoparticles. The scale bar is 200 nm.

After depositing $CH_3NH_3PbI_3$ layers on these different TiO_2 layers, we measure the surface morphology of the perovskite layers, as shown in Fig. 2. All of these $CH_3NH_3PbI_3$ layers have compact structure, but the sizes of the $CH_3NH_3PbI_3$ grains are obviously different. For the $CH_3NH_3PbI_3$ layers deposited on the TiO_2 compact layers without nanoparticles, the average size of $CH_3NH_3PbI_3$ grains is approximately 257 nm (Fig. 2(a)). By incorporating 25 nm nanoparticles into the TiO_2 layers, the average size of $CH_3NH_3PbI_3$ grains increases to 311 nm (Fig. 2(b)). Furthermore, the average sizes of $CH_3NH_3PbI_3$ grains increase to 371 nm and 381 nm for the TiO_2 layers incorporating 60 nm and 100 nm nanoparticles, respectively (Figs. 2(c) and 2(d)). Therefore, incorporating nanoparticles in the TiO_2 layers can improve the growth of $CH_3NH_3PbI_3$ grains. Figure 3 shows

the XRD patterns of four $CH_3NH_3PbI_3$ layers. Except for the diffraction peaks of FTO substrates, all the diffraction peaks can be assigned to the tetragonal phase of $CH_3NH_3PbI_3$.[31] It is also noted that the intensity of the $CH_3NH_3PbI_3$ diffraction peaks are different. By incorporating nanoparticles in the TiO_2 layers, the intensity of $CH_3NH_3PbI_3$ diffraction peaks is increased remarkably and the TiO_2 layers with 60 nm nanoparticles lead to the highest intensity of diffraction peaks. This indicates that incorporating nanoparticles in the TiO_2 layers is beneficial for the crystallization of $CH_3NH_3PbI_3$ layers and 60 nm is the optimal size of nanoparticles.

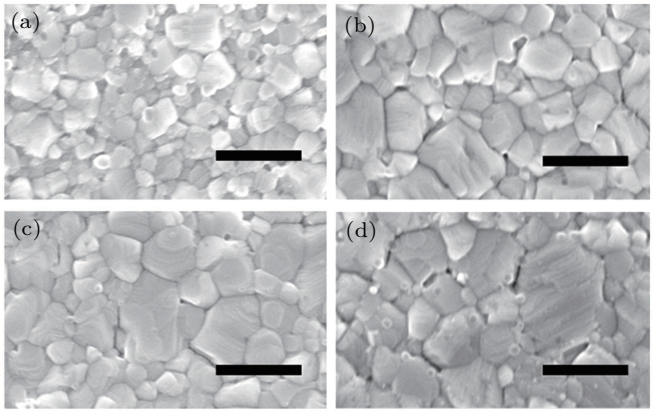


Fig. 2. Surface morphology of $CH_3NH_3PbI_3$ layers on the TiO_2 layers without (a) and with incorporation of 25 nm (b), 60 nm (c), and 100 nm (d) nanoparticles. The scale bar is 500 nm.

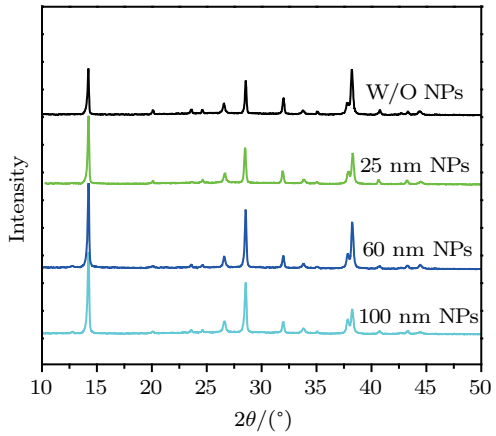


Fig. 3. (color online) XRD patterns of $CH_3NH_3PbI_3$ layers on the TiO_2 layers without (W/O NPs) and with incorporation of 25 nm (25 nm NPs), 60 nm (60 nm NPs), and 100 nm (100 nm NPs) nanoparticles.

We fabricate planar perovskite solar cells with these $CH_3NH_3PbI_3$ layers on different TiO_2 electron transport layers, and the solar-to-electric conversion performance of devices is shown in Fig. 4(a). For the TiO_2 layers without incorporating nanoparticles, the corresponding device has a PCE of 9.9% with a short-circuit current density (J_{sc}) of 16.9 mA/cm^2, an open-circuit voltage (V_{oc}) of 0.99 V, and a fill factor (FF) of 0.59. After incorporating 25 nm nanoparticles into the TiO_2 layers, the PCE increases to 12.5%, which comes from the increases in J_{sc} (18.1 mA/cm^2) and V_{oc} (1.06 V). By increasing the size of incorporated nanoparticles to 60 nm, a PCE of 16.7% is achieved with J_{sc} of 22.2 mA/cm^2 and V_{oc} of 1.10 V. However, further increasing the size of incorporated nanoparticles to 100 nm induces a decrease in PCE (15.1%) with a J_{sc} of 20.5 mA/cm^2 and V_{oc} of 1.08 V. Although efficient mesoporous devices can be easily prepared, planar devices by two-step methods usually suffer from intensive recombination and low reproducibility. These results indicate that incorporating nanoparticles can improve the TiO_2 electron transport layers and promote the performance of planar perovskite solar cells remarkably. It is noted that the optimized size of nanoparticles is 60 nm.

To confirm the superior performance of these composite electron transport layers, we compare the statistics of PCEs for the devices without and with 60 nm nanoparticles. As shown in Fig. 4(b), the TiO_2 layers with 60 nm nanoparticles lead to an average PCE of 13.6%, which is obviously better than those of devices without nanoparticles incorporation (10.1%). Figure 4(c) shows the steady-state power output of devices without and with 60 nm nanoparticles. For these two types of devices, the onset of power output has similar ramping rates. The device without nanoparticles incorporation has relatively low steady-state power output, which also degrades slightly in the 200 s measurement. The incorporation of 60 nm nanoparticles promotes the device power output significantly, and it does not degrade in the 200 s measurement. This means that incorporation of 60 nm nanoparticles is beneficial to the power output and stability of planar devices.

Figure 4(d) shows the IPCE spectra of devices with four different TiO_2 electron transport layers. All of these devices have similar IPCE values in the short-wavelength range (300–450 nm), whereas the IPCE values in the long-wavelength range (450–800 nm) are obviously different. For the devices without the incorporation of nanoparticles, the IPCE values are relatively low in the long-wavelength range, which reflects the poor collection of photogenerated electrons. After incorporating of nanoparticles with 25 nm and 60 nm in size, the IPCE values increase in the long-wavelength range continuously. However, the values of IPCE decrease markedly by further increasing the size of incorporated nanoparticles (100 nm). As the IPCE spectra can be directly related to the J_{sc} of perovskite solar cells, the trend of IPCE spectra is accordance to that of J_{sc} in Fig. 4(a). At the long-wavelength range, the penetrating depth of incident light is longer than that of short-wavelength light. Then the average transport length of photogenerated electrons is relatively long for the long-wavelength light, which leads to the difficulty of electron collection at TiO_2/perovskite interfaces. The improvement in IPCE values in Fig. 4(d) means the incorporation of TiO_2 nanoparticles can promote the electron collection process, which should be related with the electron extraction process at TiO_2/perovskite interfaces and the transport-recombination process in perovskite layers.

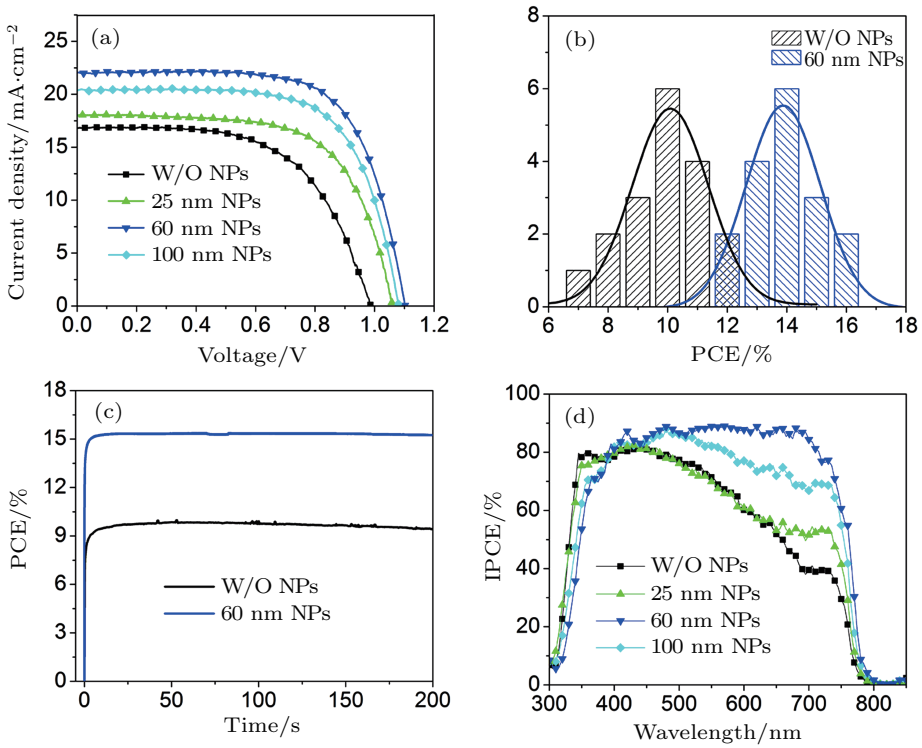


Fig. 4. (color online) Photocurrent density–photovoltage curves (a), statistics of PCEs (b), steady-state power output (c), and IPCE spectra (d) of devices with different TiO_2 electron transport layers.

PL is a facile tool for evaluating the charge extraction process at TiO_2/perovskite interfaces.[32,33] We measure the PL spectra of $CH_3NH_3PbI_3$ layers on different TiO_2 electron transport layers, and the PL spectrum of bare $CH_3NH_3PbI_3$ layers without TiO_2 layers is measured as the reference. As shown in Fig. 5, these PL peaks are located at approximately 765 nm, and their peak intensities are dependent on the properties of the TiO_2 underlayers. For the TiO_2 layers without incorporation of nanoparticles, the PL intensity of $CH_3NH_3PbI_3$ layers decrease to 63% of the intensity in bare $CH_3NH_3PbI_3$ layers. By incorporating 25 nm nanoparticles in the TiO_2 layers, the quenching effect is obviously enhanced to 17% of the PL peaks in bare $CH_3NH_3PbI_3$ layers. After increasing the size of incorporated nanoparticles to 60 nm, the PL peaks of $CH_3NH_3PbI_3$ layers can be remarkably quenched to 2.4% of the PL peaks in bare $CH_3NH_3PbI_3$ layers. As PL emission of 765 nm comes from the direct recombination of photogenerated electrons with holes in perovskite layers, the intensive quenching effect reflects the reduced density of photogenerated electrons in perovskite layers, which comes from the improved charge extraction process at the TiO_2/perovskite interfaces. However, the quenching effect attenuates slightly to 4.9% of the PL peaks in bare $CH_3NH_3PbI_3$ layers for the incorporation of 100 nm nanoparticles. Therefore, PL analysis reveals that the incorporation of 60 nm nanoparticles can improve the charge extraction process at the TiO_2/perovskite interfaces. A possible reason for this is that nanoparticles provide additional transport channels for electrons, which stimulates the electron extraction process of TiO_2 layers.

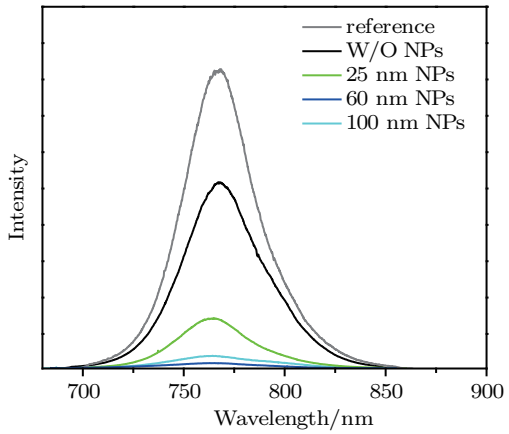


Fig. 5. (color online) PL spectra of bare $CH_3NH_3PbI_3$ layers (reference), and PL spectra of $CH_3NH_3PbI_3$ layers on TiO_2 layers without (W/O NPs) and with incorporation of 25 nm (25 nm NPs), 60 nm (60 nm NPs), and 100 nm (100 nm NPs) nanoparticles.

To investigate the transport-recombination process of perovskite solar cells, we perform the impedance measurement on the devices at 0.7 V bias potential under constant illumination. Figure 6(a) shows the Nyquist plots of devices with different TiO_2 electron transport layers, and an enlargement of the high-frequency arcs is shown in Fig. 6(b). Two arcs can be distinguished in the Nyquist plots, which can be attributed to the charge transfer process at the TiO_2/perovskite interfaces and the recombination process in perovskite layers,

respectively.[34,35] The charge transfer resistance (R_{ct}) and recombination resistance (R_{rec}) can be extracted by fitting the impedance data with the equivalent circuit in Fig. 6(a). For the devices without nanoparticle incorporation, R_{ct} is 42.9 $\Omega\cdot cm^2$ and R_{rec} is 263 $\Omega\cdot cm^2$. By incorporating 25 nm nanoparticles into the TiO_2 layers, R_{ct} decreases to 28.9 $\Omega\cdot cm^2$ and R_{rec} increases to 923 $\Omega\cdot cm^2$. For the devices with the incorporation of 60 nm nanoparticles, R_{ct} is further reduced to 16.9 $\Omega\cdot cm^2$ and R_{rec} is further promoted to 4710 $\Omega\cdot cm^2$. A low R_{ct} is beneficial to the charge transfer process at the TiO_2/perovskite interface, and a high R_{rec} is related to the low speed of the recombination process. Therefore, the incorporation of 60 nm nanoparticles in the TiO_2 layers can improve the transport-recombination process in planar perovskite solar cells. However, further increasing the size of the incorporated nanoparticles to 100 nm leads to a slight increase in R_{ct} (26.1 $\Omega\cdot cm^2$) and decrease in R_{rec} (2362 $\Omega\cdot cm^2$). Therefore, the impedance analysis indicates that the optimized size of incorporated nanoparticles is 60 nm. A low recombination process can guarantee the transport of photogenerated electrons to the TiO_2/perovskite interfaces, which is particularly important for the electrons excited by long-wavelength light.[36] This result is accordance with the *J*–*V* and IPCE measurements of these devices, as shown in Fig. 4.

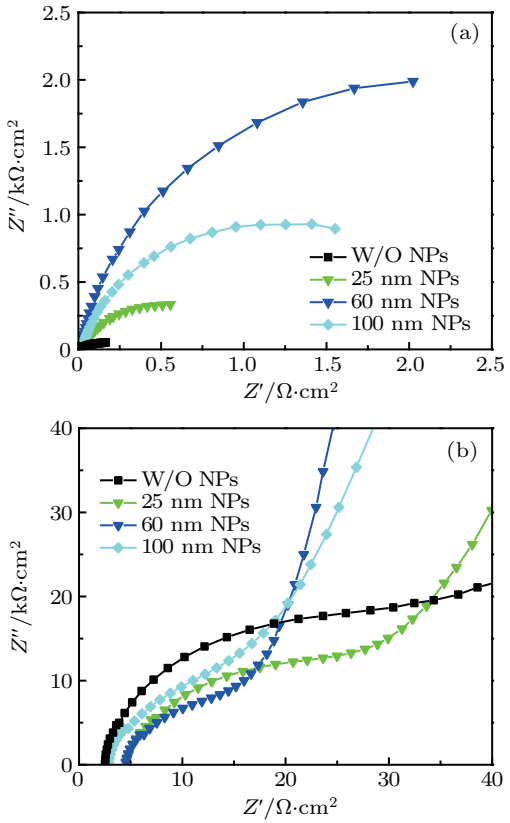


Fig. 6. (color online) Nyquist plots of devices with different TiO_2 electron transport layers (a) and the enlargement of high-frequency arcs (b).

4. Conclusion

In summary, we develop composite TiO_2 electron transport layers by a mixed spray pyrolysis method, which incorporates TiO_2 nanoparticles into the precursor solutions. We fabricate planar perovskite solar cells with these TiO_2 layers by a two-step method. It is found that the performance of these TiO_2 layers is dependent on the size of incorporated nanoparticles. For the optimized nanoparticle size of 60 nm, the PCE of the corresponding devices reaches 16.7%, which is remarkably higher than that of devices without nanoparticle incorporation (9.9%). PL and impedance measurements indicate that nanoparticles can promote the charge extraction process at the TiO_2/perovskite interfaces and improve the recombination process in perovskite layers. The convenient operation of spray pyrolysis method guarantees a promising potential for industrial application, and this mixed spray pyrolysis also can be used for other functional films.

References

[1] Kojima A, Teshima K, Shirai Y and Miyasaka T 2009 *J. Am. Chem. Soc.* **131** 6050
[2] Im J H, Lee C R, Lee J W, Park S W and Park N 2011 *Nanoscale* **3** 4088
[3] Kim H, Lee C, Im J, Lee K, Moehl T, Marchioro A, Moon S, Humphry-Baker R, Yum J, Moser J, Gr?tzel M and Park N 2012 *Sci. Rep.* **2** 591
[4] Lee M, Teuscher J, Miyasaka T, Murakami T and Snaith H 2012 *Science* **338** 643
[5] Yang W, Noh J, Jeon N, Kim Y, Ryu S, Seo J and Seok S 2015 *Science* **348** 1234
[6] Wu J, Xu X, Zhao Y, Shi J, Xu Y, Luo Y, Li D, Wu H and Meng Q 2017 *ACS Applied Materials & Interfaces* **32** 26937
[7] Yang W S, Park B W, Jung E H, Jeon N J, Kim Y C, Lee D U, Shin S, Seo J, Kim E K, Noh J H and Seok S I 2017 *Science* **356** 1376
[8] Yang G, Tao H, Qin P, Ke W and Fang G 2016 *J. Mater. Chem. A* **4** 3970
[9] Noh J, Im S, Heo J, Mandal T and Seok S 2013 *Nano Lett.* **13** 1764
[10] Wu M, Chan S, Jao M and Su W 2016 *Solar Energy Mater. Solar Cells* **157** 447
[11] Mahmud M, Elumalai N, Upama M, Wang D, Chan K, Wright M, Xu C, Haque F and Uddin A 2017 *Solar Energy Materials and Solar Cells* **159** 251
[12] Liu D and Kelly T 2014 *Nat. Photon.* **8** 133
[13] Ke W, Fang G, Liu Q, Xiong L, Qin P, Tao H, Wang J, Lei H, Li B, Wan J, Yang G and Yan Y 2015 *J. Am. Chem. Soc.* **137** 6730
[14] Baena J P C, Steier L, Tress W, Saliba M, Neutzner S, Matsui T, Giordano F, Jacobsson T J, Kandada A R S, Zakeeruddin S M, Petrozza A, Abate A, Nazeeruddin M K, Gratzel M and Hagfeldt A 2015 *Energy & Environmental Science* **8** 2928
[15] You J, Hong Z, Yang Y, Chen Q, Cai M, Song T, Chen C, Lu S, Liu Y, Zhou H and Yang Y 2014 *ACS Nano* **8** 1674
[16] Li J F, Zhao C, Zhang H, Tong J F, Zhang P, Yang C Y, Xia Y J and Fan D W 2016 *Chin. Phys. B* **25** 028402
[17] Lindblad R, Bi D, Park B W, Oscarsson J, Gorgoi M, Siegbahn H, Odelius M, Johansson E M J and Rensmo H 2014 *J. Phys. Chem. Lett.* **5** 648
[18] Zhang T H, Piao L Y, Zhao S L, Xu Z, Wu Q and Kong C 2012 *Chin. Phys. B* **21** 118401
[19] Heo J, Han H, Kim D, Ahn T and Im S 2015 *Energy & Environmental Science* **8** 1602
[20] Xia C, Song W D, Zhang C Z, Yuan S Y, Hu W X, Qin P, Wang R P, Zhao L L, Wang X F, He M and Li S T 2017 *Chin. Phys. B* **26** 018401
[21] Dualeh A, Tétreault N, Moehl T, Gao P, Nazeeruddin M K and Grätzel M 2014 *Adv. Funct. Mater.* **24** 3250
[22] Shi J, Zhang H, Xu X, Li D, Luo Y and Meng Q 2016 *Small* **12** 5288

[23] Huang A, Zhu J, Zheng J, Yu Y, Liu Y, Yang S, Bao S, Lei L and Jin P 2017 *Solar Energy Materials and Solar Cells* **163** 15
[24] Seol D, Lee J and Park N 2015 *Chem. Sus. Chem.* **8** 2414
[25] Zhou Z, Pang S, Liu Z, Xu H and Cui G 2015 *J. Mater. Chem. A* **3** 19205
[26] Wang C and Yang J 2016 *Sci. China Mater.* **59** 743
[27] Zhang R, Elzatahry A A, Al-Deyab S S and Zhao D 2012 *Nano Today* **7** 344
[28] Yuan H L, Li J P and Wang M K 2015 *Acta Phys. Sin.* **3** 038405
[29] Xia X, Li H, Wu W, Li Y, Fei D, Gao C and Liu X 2015 *ACS Appl. Mater. Interf.* **7** 16907
[30] Liu P, Yang B C, Liu G, Wu R S, Zhang C J, Wan F, Li S G, Yang J L, Gao Y L and Zhou C H 2017 *Chin. Phys. B* **26** 058401
[31] Peng Y, Jing G and Cui T 2015 *RSC Adv.* **5** 95847
[32] Shao Y, Xiao Z, Bi C, Yuan Y and Huang J 2014 *Nat. Commun.* **5** 5784
[33] Cai M, Tiong V, Hreid T, Bell J and Wang H 2015 *J. Am. Chem. Soc.* **3** 2784
[34] Juarez-Perez E, Wußler M, Fabregat-Santiago F, Lakus-Wollny K, Mankel E, Mayer T, Jaegermann W and Mora-Sero I 2014 *J. Phys. Chem. Lett.* **5** 680
[35] Zhang J, Juárez-Pérez E, Mora-Seró I, Viana B and Pauporté T 2015 *J. Mater. Chem. A* **3** 4909
[36] Xu W W, Hu L H, Luo X D, Liu P S and Dai S Y 2012 *Acta Phys. Sin.* **61** 088801